ADVANCED HEALTHCARE MATERIALS
www.advhealthmat.de

Materials Stiffness-Dependent Redox Metabolic Reprogramming of Mesenchymal Stem Cells for Secretome-Based Therapeutic Angiogenesis

*Haibo Yang, Nicole Mein Ji Cheam, Huan Cao, Melissa Kao Hui Lee, Siu Kwan Sze, Nguan Soon Tan, and Chor Yong Tay**

Cellular redox metabolism has emerged as a key tenet in stem cell biology that can profoundly influence the paracrine activity and therapeutic efficacy of mesenchymal stem cells (MSCs). Although the use of materials cues to direct the differentiation of MSCs has been widely investigated, little is known regarding the role of materials in the control of redox paracrine signaling in MSCs. Herein, using a series of mechanically tunable fibronectin-conjugated polyacrylamide (FN-PAAm) hydrogel substrates, it is shown that a mechanically compliant microenvironment with native-tissue mimicking stiffness (E = 0.15 kPa) can mechano-regulate the intracellular reactive oxygen species (ROS) level in human adipose-derived MSCs (ADMSCs). The cells reciprocate to the ROS imbalance by co-activating the nuclear factor erythroid 2–related factor 2 and hypoxia-inducible factor 1 alpha stress response signaling pathways to increase the production of vascular endothelial growth factor and basic fibroblast growth factor. Conditioned medium collected from ADMSCs grown on the 0.15 kPa FN-PAAm is found to significantly promote in vitro and ex ovo vascularization events. Collectively, these findings highlight the importance of delineating critical materials properties that can enable the reprogramming of cellular redox signaling for advanced MSCs-based secretome regenerative medicine.

1. Introduction

Mesenchymal stem cells (MSCs) hold tremendous potential for the treatment of numerous diseases.[1] As of July 2019, there are more than 900 MSCs-based clinical trials worldwide (https://clinicaltrials.gov/) that are either completed or remain in progress. A major impetus for this widespread clinical adoption of MSCs is due to their known capabilities to coordinate tissue repair responses through their paracrine activity.[2] In this regard, MSCs are also considered as a living drug store or "medicinal signaling cells" that can stimulate tissue repair through their immunomodulatory and trophic (regenerative) secretome.[3] While the diverse therapeutic effects of MSCs secretome present a huge advantage, their full clinical potential has yet to be realized as the factors and mechanisms influencing the production of MSCs secretome remain unclear.

Preconditioning MSCs could significantly improve the functions and in vivo therapeutic efficacy of MSCs by enhancing their anti-apoptotic, pro-angiogenesis, and regenerative trophic capabilities.[4] Conventional preconditioning strategies can be broadly classified as i) physiologic preconditioning (e.g., hypoxia treatment, 3D culture, etc.),[5] ii) biochemical induction (e.g., use of bioactive small molecules or drugs, etc.),[4,6] and iii) genetic manipulation.[7] Among the various preconditioning strategies, hypoxia treatment is known to promote the secretion of pro-angiogenic factors in MSCs through the activation of hypoxia-inducible factor 1 alpha (HIF1α) signaling pathway.[8] Recently, nuclear factor erythroid 2 (NFE2)-related factor (Nrf2), the redox signaling partner associated with HIF1α, was overexpressed in MSCs with the aim to improve their paracrine therapeutic efficacy for diabetic wound treatment.[9] However, the inherent molecular and microenvironmental heterogeneity of these traditional preconditioning strategies often leads to numerous undesirable off-target effects, such as cytotoxic effects and spontaneous differentiation.[10] Therefore, there is a need to innovate and develop new and cost-effective methods to precondition MSCs.

Cell-matrix interaction is known to play numerous pivotal regulatory roles in guiding stem cell fate.[11] One of the fundamental tenets of cell-matrix interaction is the integration of extracellular mechanical or solid-state signals

H. Yang, N. M. J. Cheam, H. Cao, Prof. C. Y. Tay
School of Materials Science and Engineering
Nanyang Technological University
N4.1, 50 Nanyang Avenue, Singapore 639798, Singapore
E-mail: cytay@ntu.edu.sg
M. K. H. Lee, Prof. S. K. Sze, Prof. N. S. Tan, Prof C. Y. Tay
School of Biological Sciences
Nanyang Technological University
60 Nanyang Drive, Singapore 637551, Singapore
Prof. N. S. Tan
Lee Kong Chian School of Medicine
Nanyang Technological University Singapore
11 Mandalay Road, Singapore 308232, Singapore
The ORCID identification number(s) for the author(s) of this article can be found under https://doi.org/10.1002/adhm.201900929.

DOI: 10.1002/adhm.201900929

via the process of mechanotransduction.[12] Coupled with the recent realization of the therapeutic importance of MSCs secretome, the biomaterials science community has recently started to examine the effects of extracellular matrix (ECM) or substrate cues on the paracrine activities of MSCs. For instance, the use of electrospun polycaprolactone fibers was shown to modulate the paracrine function of adipose-derived mesenchymal stem cells (ADMSCs) to promote wound healing.[13] Along the same vein, we had previously revealed that the matrix stiffness is a potent regulator of human bone marrow–derived mesenchymal stem cells (BMSCs) secretome production.[14] Among the 42 cytokines screened, secretion of 15 cytokines were observed to be significantly modulated as a function of substrate stiffness. Conditioned medium (CM) harvested from the BMSCs cultured on the mechanically compliant substrates was shown to display excellent tissue repair capability in a full thickness wound model in C57BL/6J (wildtype) mice. Taken together, these studies clearly demonstrated the profound effects of the culture microenvironment on the paracrine activity of MSCs, and therefore manipulating the culture microenvironment could potentially be exploited as a novel approach to precondition MSCs. However, the exact mechanism and signal transduction pathways that are implicated in these materials-modulated MSCs paracrine activity remain elusive.

In this study, we examined the role of substrate stiffness as a potential modulator of the MSCs redox metabolism and secretion of pro-angiogenic factors. Human telomerase reverse transcriptase (hTERT) immortalized ADMSCs were chosen as a bona fide stable MSCs model with the potential for further large-scale manufacturing of its molecular derivatives. Compared with primary MSCs, hTERT immortalized ADMSCs are more robust and have unlimited growth potential while retaining its multipotency (Figure S1, Supporting Information). Using fibronectin-conjugated polyacrylamide (FN-PAAm) hydrogels with tunable Young's modulus (E), we showed that a low material stiffness (i.e., E = 0.15 kPa) could significantly upregulate the expression of pro-angiogenic transcripts, such as vascular endothelial growth factor (VEGF) and basic fibroblast growth factor (bFGF) in ADMSCs at several magnitudes higher than conventional 3D MSCs spheroids culture.[15] At the mechanistic level, we showed that the 0.15 kPa hydrogel could alter the redox metabolism of ADMSCs, which is manifested by an overproduction of intracellular reactive oxygen species (ROS), as well as the activation of the Nrf2 stress response and HIF1α signaling pathway, leading to the induction of a "pseudohypoxic" state in ADMSCs. As a proof-of-concept, application of the CM collected from ADMSCs culture on the 0.15 kPa FN-PAAm substrate significantly enhanced endothelial cells proliferation, migration, in vitro endothelial tube network formation as well as functional angiogenesis in ex ovo chorioallantoic membrane (CAM) assay. Taken together, our results represent a first-in-class matrix rigidity-driven HIF1α response in ADMSCs under normoxic conditions, which could provide critical insights into the rational design of future development of MSCs secretome modulating substrates for targeted "cell-free" therapeutic applications.

2. Results and Discussion

2.1. PAAm Hydrogel Characterization and Behavior of ADMSCs Cultured on Hydrogel

Cytocompatible PAAm hydrogels with bio-mimicking stiffness are ideal platforms to examine the mechanobiology of adherent cells.[11,14] Shown in **Figure 1**a, is the plot of the complex modulus G^* as a function of frequency of the various PAAm hydrogels used in this study. The Young's modulus, E, was calculated from the measured average value of G^* using the expression $E = 2G^*(1 + \nu)$, where the Poisson ratio, ν, is taken to be 0.45 for PAAm hydrogel.[14] The computed E of the model PAAm hydrogels used in this study are 0.15 and 10 kPa. In comparison, glass coverslip (CS) has an E in the stiffness range of GPa. In order to promote cell adhesion on the ultralow fouling PAAm surface, *N*-sulfosuccinimidyl-6-[4'-azido-2'-nitrophenylamino] hexanoate (sulfo-SANPAH) crosslinker was used to conjugate human plasma derived fibronectin onto the PAAm hydrogel substrate (Figure S2, Supporting Information). After 48 h of culture in serum-free culture medium, it was observed that the spreading area of the ADMSCs grown on the FN-PAAm hydrogel substrates was significantly reduced as compared to the FN-coated CS control (Figure 1b). The approximated mean spreading area of the cells was 425 and 2393 μm^2 for the 0.15 and 10 kPa hydrogel substrate groups, respectively. On the other hand, spreading area of the cells grown on the extremely stiff CS was 3719 μm^2, which is significantly larger than the FN-PAAm groups by as high as eightfold. Moreover, cells grown on the CS developed prominent micron-thick stress fibers and elongated vinculin-containing focal adhesion (FA) micro-plaques (Figure 1c). In contrast, the well-developed stress fibers bundles and FAs were conspicuously absent in the cells grown on the FN-PAAm hydrogels. Furthermore, development of numerous thin filopodia-like cellular processes (white arrows) was evident on the cells grown on the hydrogels, suggesting that the cells were actively probing their immediate surroundings in search of an anchorage point (Figure 1c).[16] The decrease in cell spreading and the accompanying loss of stress fibers of the cells in the FN-PAAm groups are classical hallmarks of cells with reduced actomyosin generated tension.[17]

2.2. Role of Materials Stiffness and Cell Spreading on Cellular Redox Status

Next, we examined the effect of materials stiffness on the cellular redox status in ADMSCs. ROS metabolism has emerged as a key regulator of stem cells fate.[18] Additionally, ROS signaling transduction is also a common feature in various preconditioning methods, including but not limited to hypoxic preconditioning, TNFα treatment, and 3D cell culture.[15,19] In this study, the cellular redox status of ADMSCs was evaluated using CellRox Orange, which can produce an intense fluorescent signal when it encounters a highly oxidized environment. Interestingly, the expression level of intracellular ROS in ADMSCs was observed to be inversely correlated to

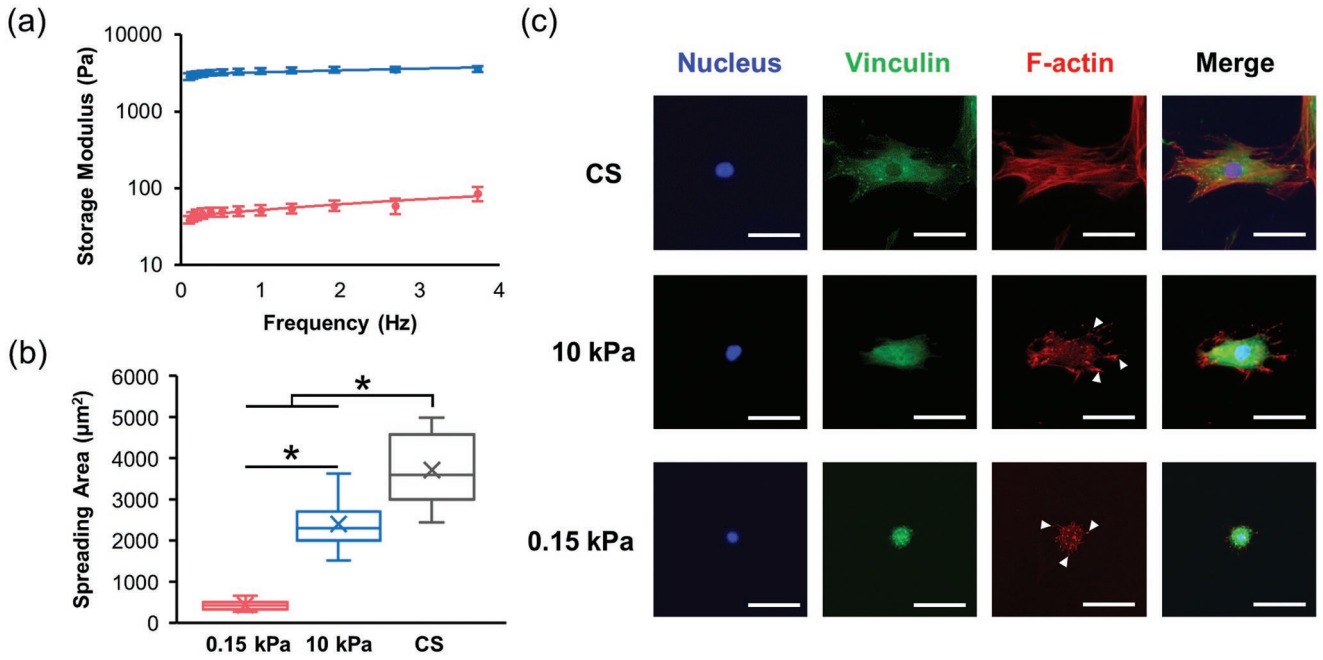

Figure 1. Characterization of PAAm hydrogel, spreading, and cytoskeleton development of ADMSCs. a) Scatterplot of storage modulus versus frequency of the PAAm hydrogels substrates obtained at a fixed shear strain of 1%, presented as mean ± SD with trendline fitting (n = 5 per group). b) Box and whisker plots of the cell spreading area on different substrates, analyzed by one-way ANOVA with Games–Howell method as post hoc test ($n \geq 30$ per group). c) Representative immunofluorescence images of cells cultured on the various substrates. Cells were counterstained for nucleus (blue), vinculin (green), and F-actin (red), with white arrows pointing to filopodia. Scale bar = 50 μm. * denotes statistical difference at $p < 0.05$.

the materials stiffness in serum-deprived culture condition (**Figure 2**a). The measured intracellular ROS levels of the cells grown on the 10 and 0.15 kPa FN-PAAm hydrogels were approximately 1.2 and 3.5 times higher (Figure 2b) than that of the cells cultured on the FN-coated CS. Since serum deprivation was reported to enhance ROS production in several cell lines via the activation of reactive oxygen species modulator 1 (Romo1), we ask whether if such materials stiffness triggered increase ROS level in ADMSCs is conditional on the level of serum.[20] However, after repeating the experiment in serum-containing (i.e., 10% fetal bovine serum) medium, we observed that the 0.15 kPa hydrogel culture substrate could similarly enhance the expression of ROS in ADMSCs as opposed to the FN-coated CS group (Figure 2c). This suggests that the materials stiffness is the predominant physical modulator of the redox status in ADMSCs, in a manner that is independent of serum level. Next, the correlation between higher levels of intracellular ROS and decrease in cell spreading was further scrutinized by means of micro-contact printing (μCP). Our μCP technology enables us to decouple the relative contribution of both cell spreading and substrate stiffness in relation to the regulation of ROS in the cells.[21] In this study, the size of the cells was systematically varied while keeping the cell shape and stiffness of the PAAm hydrogel substrate stiffness constant (i.e., 10 kPa) (Figure 2d). Cells coerced to take on a circular pattern with diameter of 60 μm were observed to express higher level of intracellular ROS (≈1.5-fold) as opposed to circular cells with a 100 μm diameter (Figure 2e). Therefore, by limiting cell spreading on the 10 kPa PAAm substrate that was previously shown to have marginal intracellular ROS-inducing effect, we were able to further augment the intracellular ROS level by suppressing cell spreading (Figure 2d,e). Our observation is consistent with a previous study, showing that limiting cell spreading by phalloidin treatment could similarly enhance intracellular ROS generation in dermal fibroblast.[22] Taken together, our results suggest that the biophysical regulation of ROS homeostasis in ADMSCs can be attributed to the reduction of cell spreading and the lowering of cellular tension on the hydrogel substrates.

2.3. Effect of Cell Substrate Stiffness on Nrf2 Stress Response in ADMSCs

In general, the increased intracellular ROS level is an indication that the cells are under oxidative stress. Therefore, we next turn our attention to the expression level of the redox-responsive transcription factor Nrf2. The Nrf2-Keap1 signaling axis is the master regulator of redox homeostasis and plays an important cytoprotective role to coordinate adaptive cellular response to oxidative stress.[23] Under basal condition, the Nrf2 binds with the Kelch-like ECH-associated protein 1 (Keap1) to form a complex that is polyubiquitinated and gets rapidly degraded by the proteasome.[24] However, exposure to elevated levels of ROS modifies the cysteine in Keap1, which can lead to the uncoupling of the Nrf2–Keap1 complex. This allows the Nrf2 to evade ubiquitination and translocate into the cell nucleus to initiate the antioxidant defense response. Although the intracellular ROS level is higher in the 10 kPa group relative to the CS control group, we did not observe any significant difference in

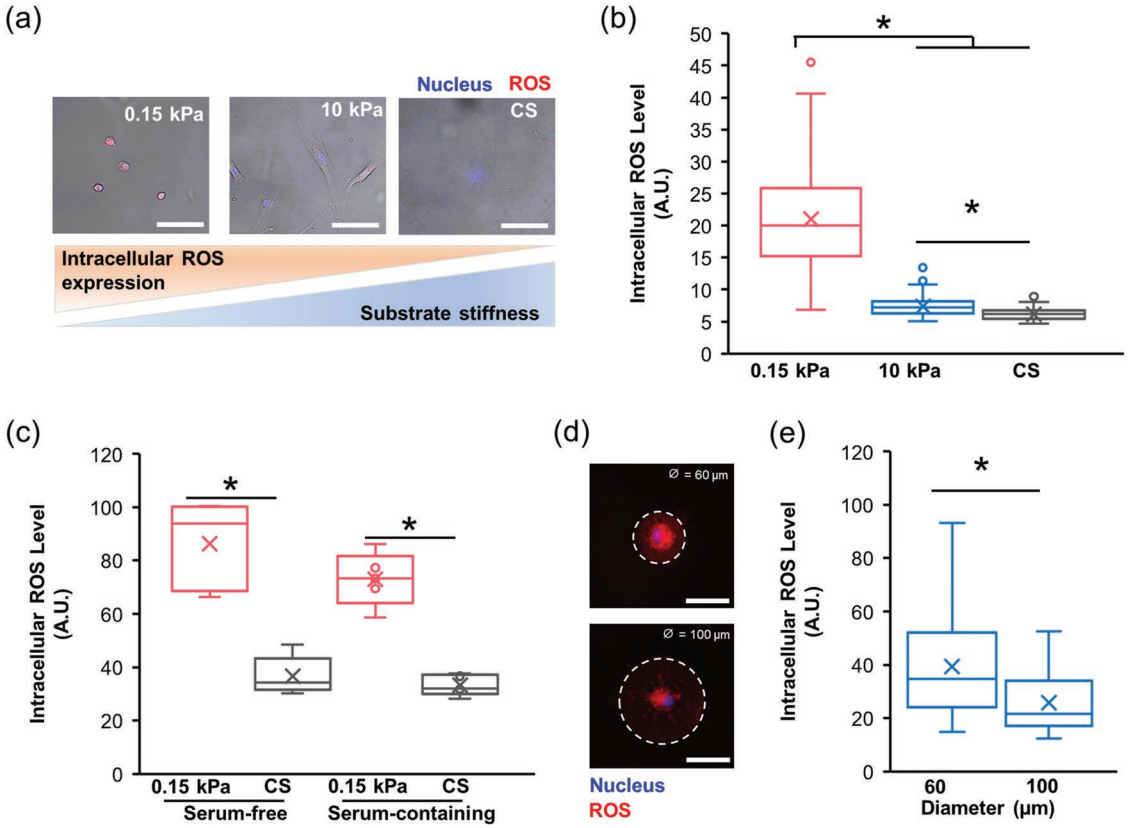

Figure 2. Materials stiffness regulates the redox status of ADMSCs. a) Representative fluorescence images and b) box and whisker plots of intracellular ROS level in ADMSCs cultured on substrate of various stiffness, analyzed by one-way ANOVA with Games–Howell method as post hoc test ($n \geq 30$ per group). Scale bar = 100 μm. c) Box and whisker plots of intracellular ROS expression level as a function of substrate stiffness and serum availability, analyzed by one-way ANOVA with Games–Howell method as post hoc test ($n \geq 30$ per group). For all images, cells are counterstained for nucleus (blue) and ROS (red). d) Representative fluorescence images and e) box and whisker plots of intracellular ROS level of micropatterned cells on FN islands of 60 and 100 μm in diameter, analyzed by one-way ANOVA ($n \geq 30$ per group). Scale bar = 50 μm. * denotes statistical difference at $p < 0.05$.

the intracellular Nrf2 expression level between the two experimental groups (**Figure 3**a,b). Conversely, enhanced expression of both cytosolic and nucleus-translocated Nrf2 was evident for cells cultured on the 0.15 kPa FN-PAAm hydrogel (Figure 3a). Specifically, the measured intranuclear Nrf2 level of the cells grown on the 0.15 kPa FN-PAAm hydrogel was observed to be ≈3 times higher than the cells cultured on the CS (Figure 3b). We also observed a coordinated upregulation of several downstream targets of Nrf2, such as heme oxygenase-1 (HMOX1), UDP glucuronosyltransferase family 1-member A1 (UGT1A1), superoxide dismutase 2 (SOD2), and NAD(P)H: quinone oxidoreductase 1 (NQO1) in the 0.15 kPa group (Figure 3c). Modulation of the cellular antioxidant potential was further examined using the total antioxidant capacity (TAC) assay. As shown in Figure 3d, while the mean TAC of the FN-coated CS group is around 0.37 mmol g^{-1}, the measured mean TAC values of the cells grown on the FN-PAAm substrates are 1.11 and 1.83 mmol g^{-1} for the 10 and 0.15 kPa group, respectively, which are significantly (three to fivefold) higher than the FN-coated CS group. Taken together, the distinctive concomitant enhancement of ROS expression, activation of Nrf2 antioxidant pathway, and increased TAC of ADMSCs cultured on the 0.15 kPa FN-PAAm, strongly suggest that the redox metabolism of ADMSCs can be mechano-regulated.

2.4. Effect of Substrate Stiffness on HIF1α Signaling and Angiogenic Potential of ADMSCs

The persistent overexpression of ROS and activation of the Nrf2 stress response have led to the speculation that other downstream targets of ROS signaling may be implicated. HIF1α is traditionally known to be a key transcriptional regulator of cellular and developmental response to hypoxia.[25] Under normoxic conditions, HIF1α is hydroxylated by prolyl hydroxylase domain-containing proteins and degraded by the proteasome.[26] However, under hypoxic conditions, HIF1α is stabilized and forms a heterodimer with HIF1β. HIF heterodimer acts as a pro-angiogenic transcription factor after translocating into the cell nucleus. On the other hand, there is also evidence to suggest that the Nrf2 stress response and HIF1α signaling pathways can work in concert to reinforce each other. Specifically, Nrf2 has been documented to increase HIF1α signaling via activation of thioredoxin; in turn, HIF1α can suppress thioredoxin reductase levels to strengthen Nrf2 signaling in a feedforward fashion.[27] **Figure 4**a shows the immunofluorescence analysis of HIF1α expression in ADMSCs that were grown on the various substrates under normoxic culture conditions. As expected, the expression level of the HIF1α was negligible in the cells cultured on the FN-coated CS.

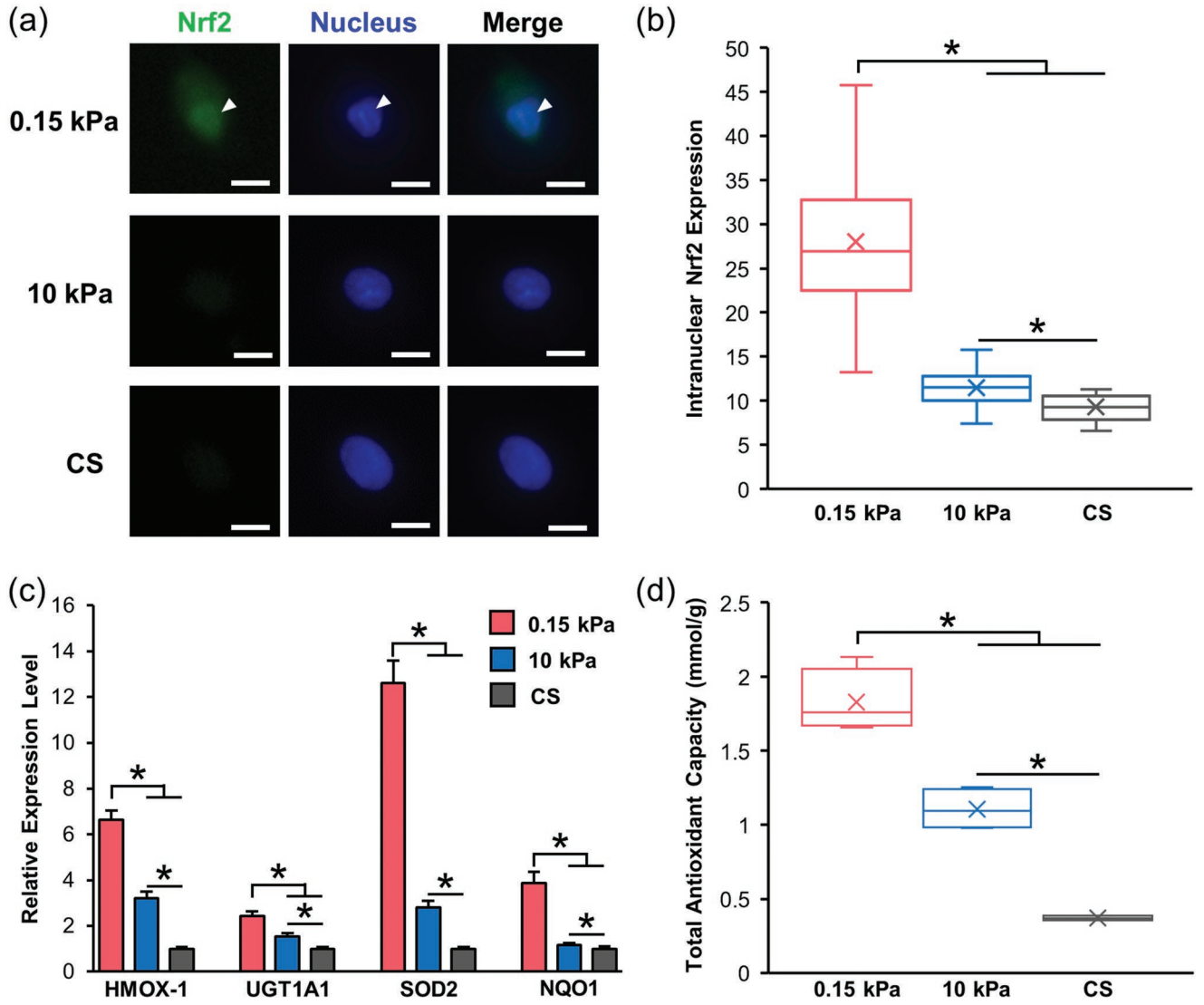

Figure 3. Materials stiffness-mediated activation of the Nrf2 stress response in ADMSCs. a) Representative immunofluorescence images and b) box and whisker plots of intranuclear Nrf2 expression of ADMSCs preconditioned on various substrates, analyzed by one-way ANOVA with Games–Howell method as post hoc test. Cells were counterstained for nucleus (blue) and Nrf2 (green) ($n \geq 30$ per group). Scale bar = 10 µm. c) Bar plots of relative expression of various downstream Nrf2-triggered antioxidant mRNA transcripts as a function of substrate stiffness, presented as mean + SD and analyzed by one-way ANOVA with Games–Howell method as post hoc test. d) Box and whisker plots of total antioxidant capacity of ADMSCs cultured on various substrates, analyzed by one-way ANOVA with Games–Howell method as post hoc test ($n = 4$ per group). * denotes statistical difference at $p < 0.05$.

However, for the cells grown on the 10 kPa FN-PAAm hydrogel substrate, increased expression of HIF1α was observed to be restricted to the cell cytoplasm. In contrast, both the cytosolic and nuclear compartments were stained positive for HIF1α when the cells were grown on the 0.15 kPa FN-PAAm hydrogel. Compared to the FN-coated CS group, intranuclear HIF1α level of the cells in the 0.15 kPa group was approximately two times higher (Figure 4b). Interestingly, treating the cells with 700×10^{-6} M *N*-acetyl-L-cysteine (NAC), a potent ROS scavenger, completely negated the expression of HIF1α on the 0.15 kPa FN-PAAm hydrogel (Figure 4c). This suggests that the mechano-regulated expression of ROS is a critical upstream event, mediating the HIF1α signaling in ADMSCs on the FN-PAAm substrate. Intriguingly, the observed coordinated upregulation of ROS level, Nrf2, and HIF1α signaling activity of the stem cells on the 0.15 kPa substrate not only corroborate but also reminisce the redox molecular events that are associated with the early stages of induced pluripotent stem cells reprogramming to retain its pluripotency.[27]

We next examined the effects of substrate stiffness on the transcriptional activation of VEGF and bFGF, two of the established pro-angiogenic targets of the HIF1α.[28] Compared to the FN-coated CS control group, significant upregulation of both VEGF (>fourfold) and bFGF (>sixfold) transcripts was observed only in ADMSCs cultured on the 0.15 kPa FN-PAAm hydrogel (Figure 4d). Strikingly, compared to 3D ADMSCs spheroids culture, an established preconditioning technique to increase pro-angiogenic proteins secretion through HIF1α

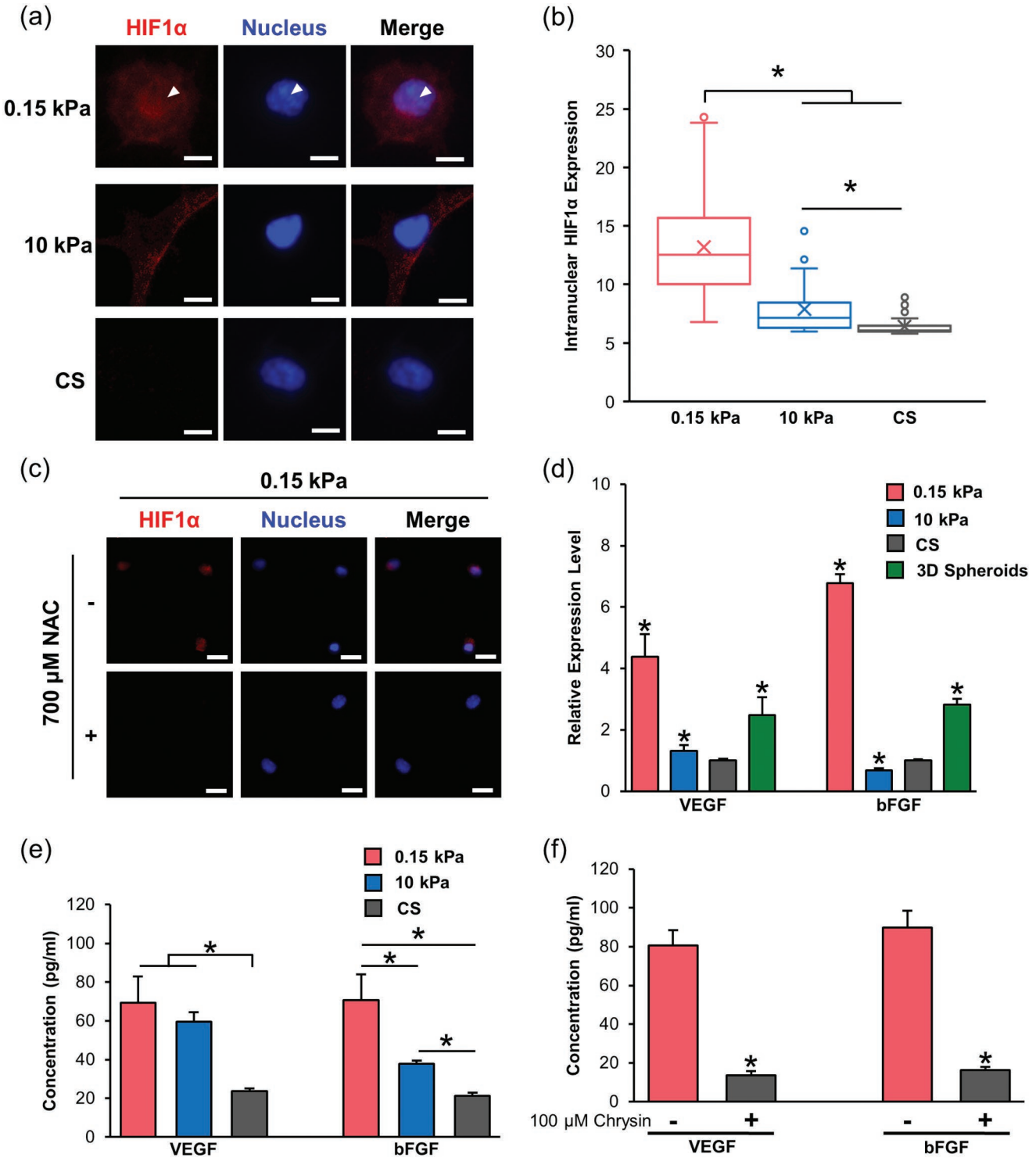

Figure 4. Materials stiffness-dependent activation of the HIF1 signaling axis. a) Representative immunofluorescence images and b) box and whisker plots of intranuclear HIF1α expression of ADMSCs preconditioned on various substrates, analyzed by one-way ANOVA with Games–Howell method as post hoc test ($n \geq 30$ per group). Scale bar = 10 μm. Cells were counterstained for HIF1α (red) and nucleus (blue). c) Representative immunofluorescence images of cells to probe for HIF1α expression on 0.15 kPa substrate treated with and without NAC (700×10^{-6} M). Scale bar = 20 μm. d) Bar plots of relative expression level of VEGF and bFGF mRNA transcripts of ADMSCs under various culture conditions, presented as mean + SD and analyzed by one-way ANOVA with Games–Howell method as post hoc test. e) Bar plots of VEGF and bFGF secretion by ADMSCs on substrates of various stiffness, presented as mean + SD and analyzed by one-way ANOVA with LSD method as post hoc test ($n = 2$ per group). f) Bar plots of VEGF and bFGF secretion by ADMSCs on 0.15 kPa FN-PAAm hydrogel with or without 100×10^{-6} M chrysin treatment (HIF1α inhibition), presented as mean + SD and analyzed by one-way ANOVA ($n = 2$ per group). * denotes statistical difference at $p < 0.05$.

signaling, cells grown on the 0.15 kPa FN-PAAm hydrogel yielded higher expression levels of VEGF and bFGF mRNA transcript expression (Figure 4d).[15] Consistent with our quantitative polymerase chain reaction (qPCR) analysis, the levels of secreted VEGF and bFGF cytokines were also observed to be significantly higher for ADMSCs grown on the 0.15 kPa substrate, which is approximately up to three times more relative to the FN-coated CS group (Figure 4e). To gain additional molecular insights into the role of HIF1α signaling and production of substrate-mediated angiogenic cytokines, we used chrysin (100×10^{-6} M), a naturally occurring antioxidant flavonoid to inhibit HIF1α signaling activity in ADMSCs (Figure S3, Supporting Information).[29] We observed that chrysin (100×10^{-6} M) treatment inhibited amount of secreted VEGF and bFGF for ADMSCs grown on the 0.15 kPa FN-PAAm substrate (Figure 4f). This strongly implies that HIF1α activity is a pivotal signaling node in our materials stiffness-mediated phenomenon. Similarly, treating the cells with NAC (700×10^{-6} M) was found to suppress the secretion of VEGF and bFGF for ADMSCs grown on 0.15 kPa FN-PAAm hydrogel (Figure S4, Supporting Information). Collectively, our data support the notion that the angiogenic potential of ADMSCs could be enhanced by targeting the redox metabolism of stem cells.[30]

2.5. Angiogenic Effects of Mechano-Regulated ADMSCs-Derived Secretome

Sprouting angiogenesis is a phenomenon where blood vessels were formed into the portions of tissues previously devoid of blood vessels through the tightly regulated process of endothelial cells (ECs) growth, migration, and tubulogenesis.[31] Along this backdrop, the functional angiogenic potential of the secretome produced by ADMSCs was assessed by in vitro human umbilical vein endothelial cells (HUVECs) proliferation and migration assays, in vitro matrigel-capillary network-like formation assay, and ex ovo CAM angiogenesis assay. Briefly, CM from ADMSCs grown on various substrates stiffness was collected after 2 days of culture under serum-free conditions and evaluated for its angiogenic potential (**Figure 5**a). CM derived from cells grown on the 0.15, 10 kPa, and CS are denoted as $CM_{0.15\ kPa}$, $CM_{10\ kPa}$, and CM_{CS}, respectively. Among the panel of CM screened, only $CM_{0.15\ kPa}$ was observed to promote the proliferation of HUVECs by approximately 20% relative to the serum-free medium (SFM) control group (Figure 5b), corroborating with our earlier findings showing 0.15 kPa is the only material stiffness that was able to activate the HIF1α signaling in ADMSCs (Figure 4a,b). The CM collected from ADMSCs grown on the 0.15 kPa FN-PAAm was further examined for its chemoattractant activity using a commercialized microfluidic-based chemotaxis lab-on-chip platform and the single-cell trajectories of the HUVECs were tracked using time-lapse microscopy over a period of 6 h. As seen in Figure 5c, HUVECs displayed a robust chemotactic behavior in response to the $CM_{0.15\ kPa}$ gradient. In contrast, directed migration of HUVECs was clearly absent in both the CM_{CS} and SFM groups. The computed chemotactic index was negligible between CM_{CS} and SFM (31.2 vs 27.9), but the chemotactic index of $CM_{0.15\ kPa}$ is significantly higher to the SFM control by approximately 2.4-fold (66 vs 27.9).

The functional angiogenic effects of the CM were further investigated by performing both the in vitro endothelial cell tube formation assay as well as the ex ovo CAM assay. As shown in Figure 5d, the formation of the well-developed tubular network was clearly visible for HUVECs that were treated with $CM_{0.15\ kPa}$, whereas SFM and CM_{CS} were less effective in inducing endothelial tube formation. Cells exposed to $CM_{0.15\ kPa}$ were able to develop an average of 140 nodes, whereas cells treated with CM_{CS} and SFM have an average node count of 100 and 80, respectively. In addition, the average tube length of the $CM_{0.15\ kPa}$-treated endothelial cells was significantly greater compared to the CM_{CS} and SFM group. Finally, the angiogenic potency of the different CM variants was evaluated by exposing 11 day old embryos to a CM-coated CS, and the corresponding patterns of blood vessels development were scored after 3 days post-treatment (Figure 5e). Consistently, we observed that an extensive network of blood vessels was formed surrounding the $CM_{0.15\ kPa}$ sample, while blood vessels formation in the CM_{CS} and SFM samples were less developed and sparse. Compared with the SFM, $CM_{0.15\ kPa}$ enhanced the development of blood vessels with an ≈1.2-fold increase of blood vessels length and an ≈1.6-fold increase of node number. Our results are consistent with earlier studies, in which the activation of HIF1α signaling in MSCs via hypoxic preconditioning was able to promote production of secretome with augmented angiogenic efficacy.[19,32] However, in our case, we demonstrate that it is also possible to engage the HIF1α signaling axis under normoxic conditions by merely using materials stiffness to induce a "pseudohypoxic state" in ADMSCs and to enhance its angiogenic activity.

3. Conclusions

In summary, we showed that materials stiffness is able to serve as a potent biophysical cue to reprogram the redox metabolism and conditional activation of the HIF signaling of ADMSCs under normoxic conditions (**Figure 6**). On conventional culture substrate with high *E*, such as glass or tissue culture treated plastics, ADMSCs maintain a basal (low) level of intracellular ROS, as well as the rapid degradation of the hydroxylated HIF1α and Nrf2-Keap1 complex by the ubiquitin-proteasome system (Figure 6a).[23,25] In contrast, on the mechanically compliant substrates, the expression of intracellular ROS level is significantly enhanced via a mechanotransduction mechanism that has yet to be fully uncovered. This resulting ROS imbalance then activates the Nrf2-ARE signaling pathway to induce the antioxidant defenses.[23] However, due to the microenvironmental condition imposed by the substrate, the Nrf2 stress response and the altered TAC are unable to fully restore redox homeostasis in ADMSCs (dashed line). As a result, the ROS level is sustained at an elevated level throughout the whole experimental time frame of 48 h. Consequently, this leads to the engagement of the ROS-dependent noncanonical HIF signaling axis and upregulates the production of angiogenic factors (Figure 6b).[33] Taken together, our findings point toward the

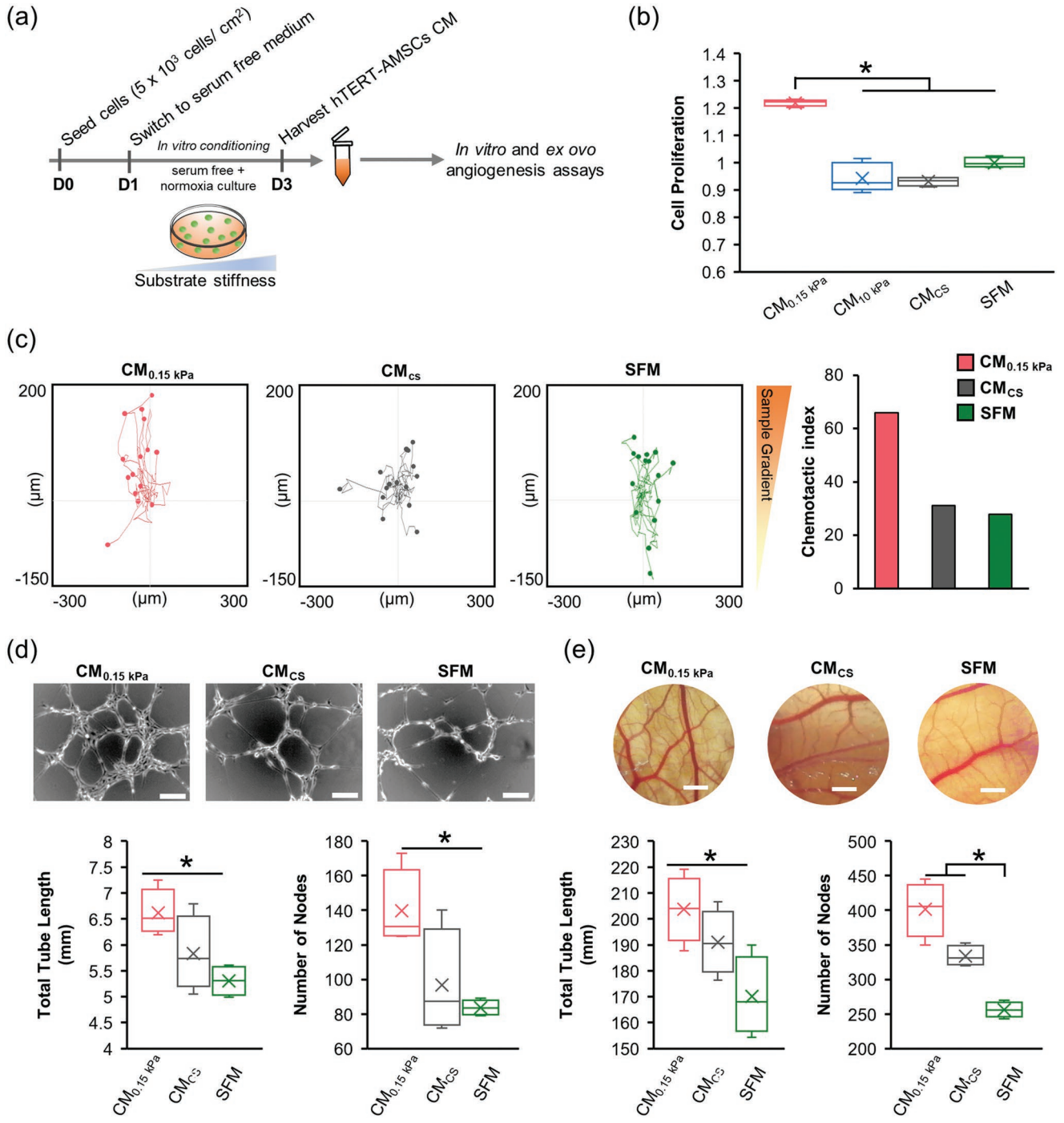

Figure 5. In vitro conditioning of ADMSCs on 0.15 kPa FN-PAAm hydrogel substrate enhances production of pro-angiogenic secretome. a) Schematic illustrating the design of the experiment ($n = 4$ per group). b) Box and whisker plots of cell proliferation measurement of HUVECs treated with ADMSCs CM under various culture conditions, analyzed by one-way ANOVA with Games–Howell method as post hoc test. c) Single cell level tracking of HUVECs migration toward the CM gradient over 6 h, with bar plots of chemotactic index presented as mean ($n = 15$ per group). Functional angiogenic potential of hTERT-AMCs secretome was evaluated using d) in vitro HUVECs tube formation assay, presented as box and whisker plots and analyzed by one-way ANOVA with LSD method as post hoc test ($n = 4$ per group; scale bar = 100 µm), and e) ex ovo CAM assay, presented as box and whisker plots and analyzed by one-way ANOVA with LSD method as post hoc test ($n = 4$ per group; scale bar = 1 mm). * denotes statistical difference at $p < 0.05$.

potential exploitation of materials stiffness to target the HIF signaling axis, without recourse to the use of soluble factors to modulate the secretion of pro-angiogenic factors in ADMSCs. The molecular insights gained in this study is posited to have a significant impact on the creation of the next-generation advanced biomaterials to tailor stem cell paracrine activity for regenerative medicine and emerging stem-cells manufacturing technologies.

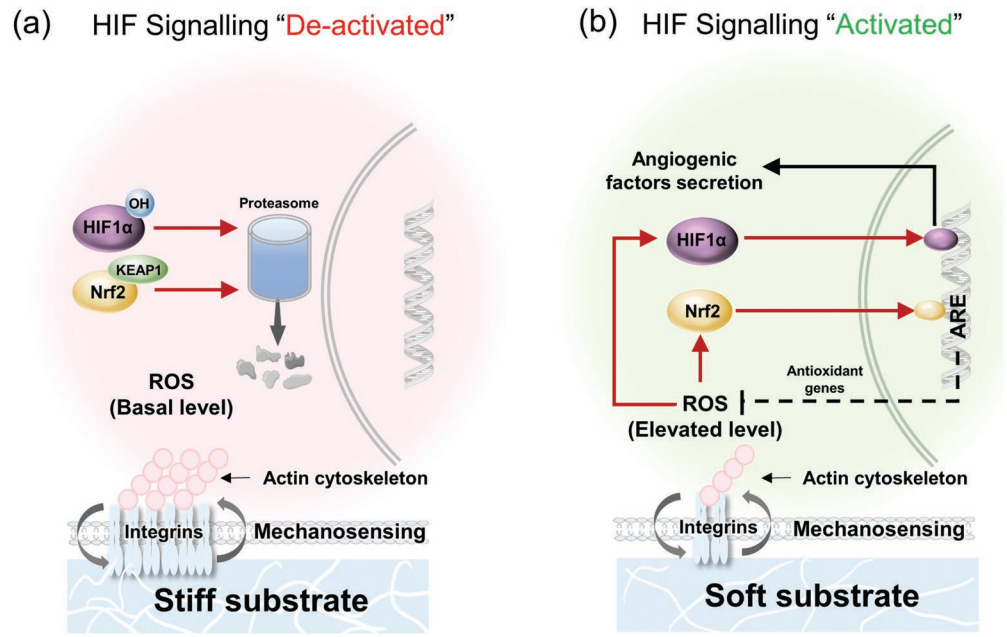

Figure 6. Proposed model of substrate stiffness functioning as a biophysical regulator of HIF-signaling in ADMSCs under normoxic conditions.

4. Experimental Section

Preparation and Characterization of PAAm Hydrogel for MSCs Preconditioning: PAAm hydrogel substrates were prepared as described previously.[14] Briefly, 22 × 22 mm square No. 1 glass CS was cleaned with ethanol and acetone prior to surface treatment using a silane working solution containing a mixture of 10 µL γ-methacryloxyprop yltrimethoxysilane, 200 µL of acetic acid, 1.8 mL of deionized (DI) water, and 8 mL of ethanol. The stiffness of the PAAm hydrogel was controlled by varying the amount of acrylamide monomer (Biorad #1610140) and bis-acrylamide monomer (Biorad #1610142) in DI water. In this study, acrylamide:bis-acrylamide weight percentage of 4%:0.15% and 10%:0.1% were used, with 0.4% ammonium persulfate and 0.04% tetramethylethylenediamine as polymerization initiator. The mixed solution was sandwiched between the surface-treated CS and a transparent plastic sheets to fabricate PAAm hydrogel on CS. Thereafter, the PAAm-coated CS was washed thoroughly for three times with pH 8.5 50×10^{-3} M HEPES (4-(2-hydroxyethyl)-1-piperazineethanesulfonic acid) buffer. Next, 350 µL of 0.5×10^{-3} M sulfo-SANPAH (ProteoChem #c1111) was dropped onto each PAAm hydrogel and UV (365 nm) irradiated for 15 min to enable conjugation of ECM protein onto the PAAm hydrogel. Residual sulfo-SANPAH was removed by washing thrice with HEPES buffer. Surface-activated PAAm hydrogel was incubated with 50 µg mL^{-1} human plasma-derived fibronectin (Merck #341635) overnight at 4 °C. FN-PAAm were washed with phosphate-buffered saline (PBS) once more to remove residual fibronectin before cell seeding. The storage modulus of the PAAm hydrogels was measured using MCR501 rheometer from Anton Paar, with a shear strain of 1% and a frequency range from 0.1 to 3.72 Hz. Successful conjugation of fibronectin to the substrates was confirmed by immunofluorescence staining using anti-fibronectin antibody produced in rabbit (Sigma F3648). All substrates were first blocked with 2% bovine serum albumin (BSA, Sigma A2153) in PBS for 1 h at room temperature before incubation with primary antibody solutions (100 times diluted in the blocking buffer) overnight at 4 °C. On the next day, the samples were washed thrice with PBS and incubated with Goat anti-Rabbit Alexa Fluor 488 antibody (Thermo A-11008) at a dilution factor of 1:100 for 1 h in the dark. Fluorescence images were captured using the Zeiss Observer Z1 inverted fluorescence microscope after another three rounds of PBS washing. For negative controls, the samples were incubated with only secondary antibody, but not primary antibody.

Cell Culture, Conditioned Medium Collection, and Characterization: hTERT immortalized ADMSCs (SCRC-4000) from ATCC were cultured with MSCs basal medium (PCS-500-030) supplemented with MSCs growth kit (PCS-500-040) as instructed by the supplier. ADMSCs between passage 5 to 10 were utilized for the study. For ADMSCs secretome collection, cells were seeded on FN-PAAm hydrogel or FN-coated CS at a density of 5000 cells cm^{-2} in complete growth medium overnight. Following which, the cells were rinsed and washed thrice with PBS before culture in serum-free high glucose Dulbecco's modified eagle medium (SFM, HyClone SH30243.01) for another 48 h. At the end of culture period, the CM was retrieved and centrifuged at 2000 *g* for 5 min. The supernatant was collected and filtered through 0.22 µm syringe filter (Sartorius #16532) to remove cellular debris. The secreted amount of VEGF and bFGF was measured using commercially available VEGF and bFGF ELISA kits (Shanghai Xitang Biotech #F03060, #F00760). To ensure fair comparison, the collected CM was normalized against the dsDNA content for each of the experimental groups with the help of AccuClear Ultra High Sensitivity dsDNA Quantification Kit (Biotium 31029) according to the manufacturer's protocol.

Preparation of 3D ADMSCs Spheroids: The ADMSCs spheroids were formed using MicroTissues 3D Petri Dish micro-mold (Sigma #Z764116) as per the manufacturer's recommended protocol. Briefly, preheated 1% agarose solution was transferred into the micro-mold, which formed the complementary agarose mold bearing the micro-wells after cooling. ADMSCs were then seeded at a density of 1.5×10^6 per agarose mold. Due to the nonbiofouling backdrop of agarose, the cells were coerced to self-aggregate to form the 3D ADMSCs spheroids.

µCP on PAAm Hydrogel Substrates: FN micropatterns were transfer printed on the surface of the PAAm hydrogel as per described earlier.[21] Polydimethylsiloxane (PDMS) stamps bearing circular micropatterns with a diameter of 60 and 100 µm were first sterilized by washing with acetone and ethanol, followed by drying with nitrogen flow. 50 µg mL^{-1} fibronectin was spread onto the patterned side of the PDMS stamps and left at room temperature for 1 h to allow the fibronectin to be adsorbed onto the PDMS stamps. Excess fibronectin was removed 1 h later, and the PDMS stamps were dried using nitrogen gas. The fibronectin-coated PDMS stamps were then placed in conformal contact with the sulfo-SANPAH-treated PAAm hydrogel. PAAm hydrogels bearing the FN islands were removed from PDMS stamps, washed with PBS, and then blocked with 1% BSA in PBS. hTERT-ADMSCs were seeded on the micro-contact-printed PAAm

hydrogels at a density of 600 cells cm^{-2} in complete growth medium for 30 min before the medium was aspirated and replenished with SFM.

Immunofluorescence Staining: The cells were washed with PBS and then fixed with either 4% paraformaldehyde for 15 min at room temperature for vinculin, F-actin, and Nrf2 staining or with prechilled methanol for 20 min at −20 °C for HIF1α staining. Thereafter, the cells were permeabilized with 0.2% Triton X-100 treatment for 10 min at room temperature. Next, the cells were blocked with 2% BSA in PBS solution for 1 h at room temperature before stained with individual primary antibody overnight at 4 °C. All primary antibodies were diluted for 100 times with blocking buffer: Monoclonal mouse anti-human vinculin antibody (Merck Millipore #90227); monoclonal rabbit anti-human Nrf2 antibody (Cell Signaling Technology #12721); monoclonal rabbit anti-human HIF1α antibody (Cell Signaling Technology 36169). Following which, the samples were washed thrice with PBS and incubated with the respective secondary antibodies at a dilution factor of 1:100 for 1 h in the dark: Chicken anti-Mouse Alexa Fluor 488 antibody (Thermo #A-21200); goat anti-Rabbit Alexa Fluor 488 antibody (Thermo #A-11008); goat anti-Rabbit Alexa Fluor 594 antibody (Thermo #A-11012). F-actin and nucleus were counter-stained with TRITC-conjugated phalloidin (Merck Millipore #90228) (1:100) and 4′,6-diamidino-2-phenylindole (Merck Millipore #90229) (1:1000). After the incubation period, the samples were washed thrice with PBS before mounting with FluoroShield Mounting Medium (Abcam #ab104139). Fluorescence images were captured using the Zeiss Observer Z1 inverted fluorescence microscope. All image processing and analysis were conducted using the ImageJ freeware (https://imagej.nih.gov/ij/). To inhibit the expression of HIF1α, ADMSCs were treated with 100×10^{-6} M of chrysin (Abcam #ab141230).

Intracellular ROS Measurement and Inhibition: The intracellular ROS expression of the cells was visualized and quantified using CellRoxOrange (Thermo #C10443). Briefly, ADMSCs were incubated with 5×10^{-6} M CellRoxOrange and 1 µg mL^{-1} Hoechst (Thermo #H3570) for 30 min at 37 °C. Following which, the samples were washed thrice with PBS and replenished with fresh medium. The CellROxOrange stained live cell samples were imaged using the Zeiss Observer Z1. NAC (Sigma #A9165) was used for ROS scavenging experiments. In order to avoid oxidization and degradation of NAC when in solution and exposed to air, NAC treatment protocol was optimized at a dosage of 700×10^{-6} M, with NAC solution refreshed every 12 h over the total 48 h culture period.[34,35]

TAC Measurement: The TAC of the cells was determined using the Trolox Equivalent Antioxidant Capacity (TEAC) assay (Beyotime Institute of Biotechnology S0119), which is based on the ability of the cell lysate samples to scavenge the 2,2'-azino-bis(3-ethylbenzothiazoline-6-sulfonic acid (ABTS) radical. The cationic ABTS radical ($ABTS^+$) was prepared by reacting the ABTS with the oxidizing agent that was supplied in the kit as per the manufacture's instruction. Cell lysates (100 µL) derived from the cells grown on the various substrate were obtained using sonication and added to the $ABTS^+$ solutions. The colorimetric changes at ab 734 nm were measured using a microplate reader (SpectraMax M2). The absorbance values of the cell lysates were then compared to the absorbance values of the Trolox standards. Total protein concentration of the cell lysates was measured using Micro BCA Protein Assay Kit (Thermo #23235). Final TAC measurements were presented as "mmol g^{-1}" by normalizing equivalent-Trolox amount ($\times 10^{-3}$ M) to the total level of cellular protein (mg mL^{-1}).

qPCR: The transcription of antioxidant and pro-angiogenic proteins by ADMSCs was examined using qPCR analysis. Total RNA was isolated with PureLink RNA Mini Kit (Thermo #12183018A). Synthesis of cDNA from the extracted RNA was done using iScript cDNA Synthesis Kit (Biorad #1708891) by performing the following reaction protocol on T100 Thermal Cycler: Priming for 5 min at 25 °C, reverse transcription for 20 min at 46 °C, and reverse transcriptase inactivation for 1 min at 95 °C. For qPCR experiment, KAPA SYBR FAST (Sigma #KK4618) was used and expression levels of the target mRNA transcripts were determined using the CFX Connect Real-Time PCR Detection System using the following protocol: polymerase activation and DNA denaturation at 95 °C for 30 s were followed by amplification for 40 cycles. Each cycle included 15 s of denaturation step at 95 °C for 15 and 30 s of annealing/extension and plate reading at 60 °C . Melting curve analysis was conducted by increasing the temperature from 65 to 95 °C with a 0.5 °C increment every 5 s. The sequence of the respective primers used in this study was obtained from primer bank (https://pga.mgh.harvard.edu/primerbank/) as listed in **Table 1** and synthesized by Sigma. Target genes transcription levels were calculated using the delta-delta Ct method, with β-actin serving as the housekeeping gene.

Table 1. Primer sequence of genes used in qPCR studies.

Gene	Primer sequence [5′-3′]	Amplicon size [bp]
HMOX-1	Forward: AAGACTGCGTTCCTGCTCAAC Reverse: AAAGCCCTACAGCAACTGTCG	247
UGT1A1	Forward: CATGCTGGGAAGATACTGTTGAT Reverse: GCCCGAGACTAACAAAAGACTCT	214
SOD2	Forward: GCTCCGGTTTTGGGGTATCTG Reverse: GCGTTGATGTGAGGTTCCAG	92
NQO1	Forward: GAAGAGCACTGATCGTACTGGC Reverse: GGATACTGAAAGTTCGCAGGG	196
VEGF	Forward: AGGGCAGAATCATCACGAAGT Reverse: AGGGTCTCGATTGGATGGCA	75
bFGF	Forward: AGAAGAGCGACCCTCACATCA Reverse: CGGTTAGCACACACTCCTTTG	82
β-actin	Forward: CATGTACGTTGCTATCCAGGC Reverse: CTCCTTAATGTCACGCACGAT	250

In Vitro HUVECs Bioassays: Primary HUVECs (Merck #SCCE001) were cultured in EndoGRO-LS Complete Culture Media Kit (Merck #SCME001). Medium changes were carried out every other day and cells from passages 10 to 12 were used in in vitro HUVECs bioassays.

CM collected from ADMSCs grown on the various substrates was mixed with EndoGRO-LS Complete Culture Medium at an optimized mixing ratio of 30:70 and used for in vitro HUVECs proliferation studies. HUVECs were unable to survive in pure SFM and a minimal amount (70%) of EndoGRO-LS Complete Culture Medium was needed to keep the cells viable. HUVECs suspended in EndoGRO-LS Complete Culture Medium were first seeded into 96-well plate at a density of 5000 cells cm^{-2}. On the following day, the complete culture medium was replaced by the CM mixtures and the cell proliferation was determined 48 h later using the PrestoBlue (Thermo #A13262) metabolic assay.

The effect of ADMSCs' secretome on the migratory capacity of HUVECs was examined using the µ-Slide Chemotaxis (ibidi #80306) in accordance to the manufacturer's protocol. Specific to this study, a seeding density of 1.8×10^4 HUVECs per chip was used. To establish the chemotactic gradient, 18 µL of the various CM mixture was introduced in the upper chamber while the lower chamber was infused with SFM. Following which, the migratory behavior of the HUVECs was monitored over a period of 6 h using the JuLI Stage Real-Time Cell History Recorder (NanoEntek). For each group, the migratory tracks of 15 HUVECs were tracked manually with the Manual Tracking plugin in ImageJ. The Center of Mass (CoM) was computed with the online Chemotaxis and Migration Tool from ibid. CoM represented the spatial averaged positioning of all HUVECs endpoints for each group and it was calculated using the following expression.

$$\mathrm{CoM} = \frac{1}{n}\sum_{i=1}^{n}\left(X_{i,\mathrm{end}}, Y_{i,\mathrm{end}}\right) \quad (1)$$

Based on CoM, chemotactic index, which was derived from the *Y*-axis value of CoM, was used to quantify the extent of HUVECs migrating toward the CM mixtures.

In vitro HUVEC tube-formation assay was performed using the µ-Plate Angiogenesis 96 Well (ibidi #89646). In this study, matrigel

(Corning #356237) was first coated onto the wells of the µ-Plate. 20 000 HUVECs suspended in a mixture of 15 µL of CM and 35 µL of EndoGRO-LS Complete Culture Medium were then seeded into every well of the µ-Plate. Samples were then incubated for 3 h to allow the formation of capillary-like tube and subsequently imaged using the Zeiss Primo Vert Inverted Microscope. Bright field images were analyzed with the Angiogenesis Analyzer plugin of ImageJ. The number of nodes and total tube length was computed to quantify the extent of tube formation.

Ex Ovo CAM Assay: Fresh specific-pathogen-free chicken eggs were collected from the Agri-Food & Veterinary Authority of Singapore on embryonic day E0 and kept in 37 °C with 60% humidity to allow embryonic development. After 48 h (E2), the eggs were cracked opened, and each of the chicken embryo was transferred into an artificial culture vessel containing a plastic cup lined with a support plastic wrap to cradle the embryos. In order to prevent bacteria contamination, 100 µL of Penicillin-Streptomycin (Gibco #15140-122) was introduced to each embryo (E2) every 3 days. From E5 onward, 100 µL of 20 mg mL^{-1} $CaCl_2$ (Sigma #C5670) in DI water was applied to the embryos (E5) every 3 days. By E11, formation of the blood vessels network was clearly visible, and the chick embryos were transferred to plastic petri dishes. ADMSCs-derived CMs (10 µL) were locally administered to the developing embryo with the aid of pre-cut CS and left to incubate at 37 °C for 3 days. Thereafter, blood vessels proximal to CM-coated CS were imaged with a Plugable Digital Viewer and analyzed using ImageJ.

Statistical Analysis: All other raw data were used directly without any preprocessing. Data were either presented as mean ± SD in scatterplot with trendline fitting, as mean + SD in bar plots, or as box and whisker plots to better illustrate the variance. Statistical significance was determined by one-way analysis of variance (ANOVA) using SPSS. *F*-test was first carried out to check the homogeneity of variance, with equal variance as null hypothesis. Subsequently, least significant difference (LSD) method was used as post hoc test for equal variance while Games–Howell method was used as post hoc test for unequal variance, if applicable, with nonsignificant difference between groups as null hypothesis. Results are considered statistically significant with $p < 0.05$.

Supporting Information

Supporting Information is available from the Wiley Online Library or from the author.

Acknowledgements

The authors gratefully acknowledge the financial support from the Nanyang Technological University and the Singapore Ministry of Education - Singapore (MOE2018-T2-1-043 to C.Y.T. and N.S.T.).

Conflict of Interest

The authors declare no conflict of interest.

Keywords

materials stiffness, mesenchymal stem cells, redox metabolism, regenerative medicine, secretome

Received: July 16, 2019
Revised: August 23, 2019
Published online:

[1] C. A. Keller, T. A. Gonwa, D. O. Hodge, D. J. Hei, J. M. Centanni, A. C. Zubair, *Stem Cells Transl. Med.* **2018**, *7*, 161.
[2] V. B. R. Konala, M. K. Mamidi, R. Bhonde, A. K. Das, R. Pochampally, R. Pal, *Cytotherapy* **2016**, *18*, 13.
[3] A. I. Caplan, *Stem Cells Transl. Med.* **2017**, *6*, 1445.
[4] G. R. Linares, C.-T. Chiu, L. Scheuing, Y. Leng, H.-M. Liao, D. Maric, D.-M. Chuang, *Exp. Neurol.* **2016**, *281*, 81.
[5] a) K. H. Han, A. K. Kim, M. H. Kim, D. H. Kim, H. N. Go, D. I. Kim, *Cell Biol. Int.* **2016**, *40*, 27; b) J. E. Park, S. W. Tse, G. Xue, C. Assisi, A. S. Maqueda, G. P. X. Ramon, J. K. Low, O. L. Kon, C. Y. Tay, J. P. Tam, *Oncotarget* **2019**, *10*, 2136.
[6] E. Redondo-Castro, C. Cunningham, J. Miller, L. Martuscelli, S. Aoulad-Ali, N. J. Rothwell, C. M. Kielty, S. M. Allan, E. Pinteaux, *Stem Cell Res. Ther.* **2017**, *8*, 79.
[7] D.-D. Wang, M. Yang, Y. Zhu, C. Mao, *Biomacromolecules* **2015**, *16*, 3897.
[8] X. Hu, S. P. Yu, J. L. Fraser, Z. Lu, M. E. Ogle, J.-A. Wang, L. Wei, *J. Thorac. Cardiovasc. Surg.* **2008**, *135*, 799.
[9] X. Li, X. Xie, W. Lian, R. Shi, S. Han, H. Zhang, L. Lu, M. Li, *Exp. Mol. Med.* **2018**, *50*, 29.
[10] S. S. Ho, K. C. Murphy, B. Y. Binder, C. B. Vissers, J. K. Leach, *Stem Cells Transl. Med.* **2016**, *5*, 773.
[11] A. J. Engler, S. Sen, H. L. Sweeney, D. E. Discher, *Cell* **2006**, *126*, 677.
[12] a) X. Jia, K. Minami, K. Uto, A. C. Chang, J. P. Hill, T. Ueki, J. Nakanishi, K. Ariga, *Small* **2019**, *15*, 1804640; b) M. Oksdath, S. L. Perrin, C. Bardy, E. F. Hilder, C. A. DeForest, R. D. Arrua, G. A. Gomez, *APL Bioeng.* **2018**, *2*, 041501.
[13] N. Su, P.-L. Gao, K. Wang, J.-Y. Wang, Y. Zhong, Y. Luo, *Biomaterials* **2017**, *141*, 74.
[14] H. Yang, K. T. Nguyen, D. T. Leong, N. S. Tan, C. Y. Tay, *ACS Appl. Mater. Interfaces* **2016**, *8*, 26591.
[15] Y. Xu, T. Shi, A. Xu, L. Zhang, *J. Cell. Mol. Med.* **2016**, *20*, 1203.
[16] C. Y. Tay, H. Gu, W. S. Leong, H. Yu, H. Q. Li, B. C. Heng, H. Tantang, S. C. J. Loo, L. J. Li, L. P. Tan, *Carbon* **2010**, *48*, 1095.
[17] a) J. Li, J. Di Russo, X. Hua, Z. Chu, J. P. Spatz, Q. Wei, *Adv. Healthcare Mater.* **2019**, *8*, 1801384; b) Y. Zhukova, C. Hiepen, P. Knaus, M. Osterland, S. Prohaska, J. W. Dunlop, P. Fratzl, E. V. Skorb, *Adv. Healthcare Mater.* **2017**, *6*, 1601244.
[18] J. M. Ryu, H. J. Lee, Y. H. Jung, K. H. Lee, D. I. Kim, J. Y. Kim, S. H. Ko, G. E. Choi, *Int. J. Stem Cells* **2015**, *8*, 24.
[19] S. Bartaula-Brevik, A. Bolstad, K. Mustafa, T. Pedersen, *Int. J. Stem Cell Res. Ther.* **2017**, *4*, 2469.
[20] S. B. Lee, J. J. Kim, T. W. Kim, B. S. Kim, M.-S. Lee, Y. Do Yoo, *Apoptosis* **2010**, *15*, 204.
[21] C. Y. Tay, Y.-L. Wu, P. Cai, N. S. Tan, S. S. Venkatraman, X. Chen, L. P. Tan, *NPG Asia Mater.* **2015**, *7*, e199.
[22] C. Quan, M. K. Cho, D. Perry, T. Quan, *J. Biomed. Sci.* **2015**, *22*, 62.
[23] Z. Wu, H. Yang, G. Archana, M. Rakshit, K. W. Ng, C. Y. Tay, *Nanotoxicology* **2018**, *12*, 1215.
[24] P. Deshmukh, S. Unni, G. Krishnappa, B. Padmanabhan, *Biophys. Rev.* **2017**, *9*, 41.
[25] V. Malec, O. R. Gottschald, S. Li, F. Rose, W. Seeger, J. Hänze, *Free Radical Biol. Med.* **2010**, *48*, 1626.
[26] S. Crunkhorn, *Nat. Rev. Drug Discovery* **2016**, *15*, 309.
[27] K. E. Hawkins, S. Joy, J. M. Delhove, V. N. Kotiadis, E. Fernandez, L. M. Fitzpatrick, J. R. Whiteford, P. J. King, J. P. Bolanos, M. R. Duchen, *Cell Rep.* **2016**, *14*, 1883.
[28] D. C. Irwin, J. M. McCord, E. Nozik-Grayck, G. Beckly, B. Foreman, T. Sullivan, M. White, J. T. Crossno Jr., D. Bailey, S. C. Flores, *Free Radical Biol. Med.* **2009**, *47*, 55.
[29] B. Fu, J. Xue, Z. Li, X. Shi, B.-H. Jiang, J. Fang, *Mol. Cancer Ther.* **2007**, *6*, 220.
[30] a) M. Ushio-Fukai, N. Urao, *Antioxid. Redox Signaling* **2009**, *11*, 2517; b) F. Sharifpanah, S. Behr, M. Wartenberg, H. Sauer, *Biochim. Biophys. Acta* **2016**, *1863*, 3096.

[31] T. H. Adair, J.-P. Montani, in *Colloquium Series on Integrated Systems Physiology: From Molecule to Function* (Eds: D. N. Granger, J. P. Granger), Morgan & Claypool Life Sciences, San Rafael, CA **2010**.
[32] a) V. Razban, A. S. Lotfi, M. Soleimani, H. Ahmadi, M. Massumi, S. Khajeh, M. Ghaedi, S. Arjmand, S. Najavand, A. Khoshdel, *BioRes. Open Access* **2012**, *1*, 174; b) S. Bian, L. Zhang, L. Duan, X. Wang, Y. Min, H. Yu, *J. Mol. Med.* **2014**, *92*, 387.
[33] S. Movafagh, S. Crook, K. Vo, *J. Cell. Biochem.* **2015**, *116*, 696.
[34] M. Columbaro, S. Ravera, C. Capanni, I. Panfoli, P. Cuccarolo, G. Stroppiana, P. Degan, E. Cappelli, *PLoS One* **2014**, *9*, e104857.
[35] L. Pavliv (Cumberland Pharmaceuticals Inc.), *EP1928449B1*, **2012**.